1064–1079 *Nucleic Acids Research, 2016, Vol. 44, No. 3* *Published online 7 October 2015*
doi: 10.1093/nar/gkv1021

Chromatin association of the SMC5/6 complex is dependent on binding of its NSE3 subunit to DNA

Katerina Zabrady[1,2], Marek Adamus[1], Lucie Vondrova[1,2], Chunyan Liao[3], Hana Skoupilova[2], Marketa Novakova[2], Lenka Jurcisinova[1,2], Aaron Alt[3], Antony W. Oliver[3], Alan R. Lehmann[3] and Jan J. Palecek[1,2,*]

[1]Mendel Centre for Plant Genomics and Proteomics, Central European Institute of Technology, Masaryk University, Kamenice 5, Brno, 62500, Czech Republic, [2]Laboratory of Functional Genomics and Proteomics, National Centre for Biomolecular Research, Faculty of Science, Masaryk University, Kotlarska 2, Brno, 61137, Czech Republic and [3]Genome Damage and Stability Centre, University of Sussex, Falmer, Brighton BN1 9RQ, United Kingdom

Received December 19, 2014; Revised September 23, 2015; Accepted September 26, 2015

ABSTRACT

SMC5/6 is a highly conserved protein complex related to cohesin and condensin, which are the key components of higher-order chromatin structures. The SMC5/6 complex is essential for proliferation in yeast and is involved in replication fork stability and processing. However, the precise mechanism of action of SMC5/6 is not known. Here we present evidence that the NSE1/NSE3/NSE4 sub-complex of SMC5/6 binds to double-stranded DNA without any preference for DNA-replication/recombination intermediates. Mutations of key basic residues within the NSE1/NSE3/NSE4 DNA-binding surface reduce binding to DNA *in vitro*. Their introduction into the *Schizosaccharomyces pombe* genome results in cell death or hypersensitivity to DNA damaging agents. Chromatin immunoprecipitation analysis of the hypomorphic *nse3* DNA-binding mutant shows a reduced association of fission yeast SMC5/6 with chromatin. Based on our results, we propose a model for loading of the SMC5/6 complex onto the chromatin.

INTRODUCTION

In eukaryotes, the structural maintenance of chromosomes (SMC) family of conserved complexes contains cohesin, condensin and the SMC5/6 complex. The core of each complex is composed of a SMC heterodimer: SMC1 and SMC3 in cohesin, SMC2 and SMC4 in condensin, and SMC5 and SMC6 in the SMC5/6 complex. The SMC proteins are folded into a structure containing an ATPase head-domain at one end, an intramolecular coiled-coil region, and a hinge domain at the other end. The SMC proteins heterodimerize through their hinge domains. The non-SMC kleisin subunit bridges the head domains of SMC proteins to form a ring-like structure. The kleisin subunit usually interacts with other non-SMC subunits of the complex (1,2).

The cohesin complex mediates sister chromatid cohesion from S-phase until anaphase, whilst condensin promotes chromatin condensation during mitosis (1). Both cohesin and condensin complexes are also involved in DNA repair processes (3,4). The essential function of the SMC5/6 complex (5,6) is not clear, but it is known that it is important for both DNA damage repair and for chromatin dynamics (5). It has been shown in yeast that the SMC5/6 complex has a role in stabilization of stalled replication forks (RF) (7), in sequestering nascent chromatid intertwinings that form behind the replication machinery (8), in resolution of homologous recombination (HR) structures (9–13) and in removing of cohesin from mitotic chromosomes (14,15). In human cells, the complex is required also for DNA replication processing (16) and alternative lengthening of telomeres (17).

It has been proposed that a central feature of the SMC complexes is the entrapment of chromosomes within their ring structures (18,19). For cohesin, it has been suggested that ATP binding and hydrolysis by the SMC1/SMC3 head domains lead to the opening of the cohesin ring, probably at the SMC1/SMC3 hinge domain interface, and allow entrapment of a DNA fibre (20–22). In addition, a separate complex, Scc2/Scc4, is necessary for loading of cohesin. The Scc2/Scc4 complex, containing HEAT-repeats, binds to double-stranded DNA (dsDNA) first, then interacts with cohesin and stimulates its ATPase activity in the presence of DNA (23).

In *Saccharomyces cerevisiae* (*S. cerevisiae*) condensin, the kleisin subunit Brn1 is associated with two non-SMC subunits containing HEAT-repeats, Ycs4 and Ycg1 (24). Ycs4

*To whom correspondence should be addressed. Tel: +420 54949 5952; Fax: +420 54949 2654; Email: jpalecek@sci.muni.cz
Present address: Marketa Novakova, Biology and Diseases of Wildlife, University of Veterinary and Pharmaceutical Sciences, Palackeho tr. 1/3, Brno, 612 42, Czech Republic.

and Ycg1 physically and selectively interact with dsDNA and their binding to DNA stimulates the ATPase activity of SMC2/SMC4 proteins (24). It has been proposed that ATP hydrolysis leads to the opening of the condensin ring and enables the entry of the DNA fibre. In contrast to Ycs4/Ycg1 interaction, the SMC2/SMC4 hinge domains have been shown to bind preferentially to single-stranded DNA (ssDNA) over dsDNA, consistent with a single-strand break repair function of the condensin complex (24,25).

Similar to SMC2/SMC4 proteins, the SMC5 and SMC6 proteins preferentially bind to ssDNA, consistent with their role in DNA repair (26,27). However, it has been shown that the SMC5/6 complex ATPase activity is selectively stimulated, like condensin, by dsDNA (28). The SMC5/6 ATPase head domains interact with the NSE4 kleisin subunit, which itself forms a stable NSE1/NSE3/NSE4 (NSE1/3/4) subcomplex with NSE1 and NSE3 subunits (29–32).

In this paper, we show that the NSE1/3/4 sub-complex binds to dsDNA. The key components of this interaction are highly evolutionarily conserved basic amino acids in the C-terminal winged-helix (WH) domain of the NSE3 subunit. The NSE3–DNA interaction is essential for proliferation in fission yeast *Schizosaccharomyces pombe* (*S. pombe*) cells. Chromatin immunoprecipitation (ChIP) experiments with an *S. pombe nse3* hypomorphic mutant show reduced accumulation of SMC5/6 in chromatin, suggesting a role for the NSE3–DNA interaction in loading or maintenance of the SMC5/6 complex on yeast chromatin.

MATERIALS AND METHODS

Plasmids

pET-28c–6xHis-hNSE3(aa1–304) was provided by R. Arribas (University of Sussex, UK). pRSFDuet-1–6xHis-hNSE1(aa1–266)+hNSE3(aa1–304) (pRP318) was provided by Potts (33). To generate the pRSFDuet-1–6xHis-hNSE1(aa1–266) construct, pRP318 was cleaved using *Sal*I and *Xho*I restriction enzymes to remove the hNSE3 open reading frame (ORF). Digested plasmid containing hNSE1(aa1–266) gene was re-ligated using T4 DNA ligase (NEB).

To generate expression pRSFDuet-1–6xHis-hNSE1(aa1–266)+hNSE3(aa1–304)+Strep-hNSE4b(aa92–212) construct (KC808), the *BamH*I–*Xho*I hNSE1(aa1–266)+hNSE3(aa1–304) fragment from pRP318 was inserted into the *BamH*I–*Sal*I sites of empty pRSFDuet-1 vector (resulting in KC451). Then the hNSE4b(aa92–212) fragment was amplified with KB316 and KB319 primers (Supplementary Table S1) using an *E. coli* codon optimized pMA–hNSE4b(aa2–333) clone as a template (GeneArt Gene Synthesis, Life Technologies; template sequence in Supplementary Table S2). The PCR product containing Strep-hNSE4b(aa92–212) was then inserted into the *Eco*RV–*Xho*I digested KC451 by the In-Fusion cloning protocol (Clontech). In-Fusion cloning was used to generate all subsequent expression constructs.

pRSFDuet-1–Nse1(aa1–232)+6xHis-Nse3(aa1–328)+2xStrep-Nse4(aa1–300) (KC661) was prepared in the four following steps: (i) Nse1(aa1–232) was amplified using KB225 and KB226 primers (Supplementary Table S1). The PCR product was cloned into the *Nco*I–*Hind*III sites of pRSFDuet-1 vector (KV1). (ii) *S. pombe* Nse3 ORF was amplified with KB188 and KB189 primers and inserted into the *Nde*I–*Xho*I digested pRSFDuet-1 vector (KV2). This construct was used as a template for PCR with KB254 and KB189 primers. The 6xHis-Nse3(aa1–328) PCR product was cloned into the *Nde*I–*Xho*I sites of KV1 creating pRSFDuet-1–Nse1(aa1–232)+6xHis-Nse3(aa1–328) (KC600). (iii) KC600 was used as template for PCR amplification of Nse1(aa1–232)+6xHis-Nse3(aa1–328) with KB225 and KB190 primers. The PCR product was cloned into the *Nco*I–*Sal*I sites of empty pRSFDuet-1 vector (KV3). (iv) Nse4(aa1–300) was PCR amplified with KB191 and KB192 primers, and cloned into the *Eco*RV–*Xho*I sites of KV3 generating pRSFDuet-1–Nse1(aa1–232)+6xHis-Nse3(aa1–328)+Nse4(aa1–300) (KV4). This construct was then digested with *Eco*RV and annealed KB230 and KB231 oligonucleotides (2xStrep) were inserted in front of the *S. pombe* Nse4 ORF, creating the final pRSFDuet-1–Nse1(aa1–232)+6xHis-Nse3(aa1–328)+2xStrep-Nse4(aa1–300) construct (KC661).

The yeast two-hybrid (Y2H) pGBKT7-Smc5(aa1–323+732–1065) head construct (DB12) was described previously (29). pEPEX-Smc6(aa1–1140) (29) was *Nde*I–*Sal*I digested and Smc6 was inserted into *Nde*I–*Xho*I digested pGADT7 vector resulting in pGADT7-Smc6 (JP56). pPM587-Nse3(aa1–328)+Nse4(aa1–300)+Nse1(aa1–232) (LJ38) was prepared in three following steps: (i) To generate pPM587-Nse4(aa1–300) (KA70), the pGEM-Nse4 (29) was *BamH*I–*Eco*RI digested and the Nse4 containing fragment was inserted into the *BamH*I–*Eco*RI digested pPM587 vector using T4 DNA ligase. The Nse3 ORF was PCR amplified using JP684 and JP685 primers and inserted into the pCRII-TOPO vector (using TOPO TA cloning kit, Invitrogen) to give pCRII-Nse3 (JP334); JP334 was subsequently digested with *Eco*RI and the Nse3 ORF containing fragment was inserted into the *Eco*RI digested pPM587 vector to give pPM587-Nse3(aa1–328) (KA103), pPM587-Nse1(aa1–232) (KA67) was previously described in (32). (ii) To create KC828, the KA70 construct with KB353 and KB354 primers were used to PCR amplify the ADH1-Nse4(aa1–300)-CYC terminator fragment and the fragment was cloned into *Kpn*I digested KA103 (behind the CYC terminator) by In-Fusion cloning. (iii) KA67 with KB353 and KB354 primers were used to PCR amplify the ADH1-Nse1(aa1–232)-CYC terminator fragment. KC828 was subsequently digested with *Kpn*I and the ADH1-Nse1(aa1–232)-CYC terminator fragment was inserted into KA828 (behind the ADH1-Nse4(aa1–300)-CYC terminator fragment) to create pPM587-Nse3(aa1–328)+Nse4(aa1–300)+Nse1(aa1–232) (LJ38).

In-silico modelling and docking

The I-TASSER server (34) was used to obtain the complete human NSE3 WH-B domain structure in Figure 1A. The crystal structure of hNSE1/hNSE3 (hNSE1/3) dimer (PDB: 3NW0) served as the threading template.

For DNA docking, an 'ideal' 15 nucleotide B-form DNA duplex was generated in Coot (35). This was then docked into the crystal structure of the hNSE1/3 heterodimer

(PDB: 3NWO; previously reported by Doyle *et al.* (33)) using the 'Easy Interface' of the HADDOCK Web Docking Server (36,37) (http://www.haddock.science.uu.nl). The following amino acids were defined as 'Active' residues, hNSE1-K139, K140, R142, K144 and hNSE3-K221, R229, R237 (highlighted in green in Figure 3A), whilst 'passive' residues were automatically chosen. The 'best' structure (with a HADDOCK score of -72.6 ± 11, for a cluster size of 39, and *Z*-score of -1.8) was then used to generate Figure 3A with PyMOL (The PyMOL Molecular Graphics System, Version 1.7.2, Schrödinger, LLC; http://www.pymol.org).

Site-directed mutagenesis

The QuikChange Lightning Site-Directed Mutagenesis Kit (Agilent Technologies) was used to create point mutations in the pRSFDuet-1–6xHis-hNSE1(aa1–266)+hNSE3(aa1–304)+Strep-hNSE4(aa92-212), pRSFDuet-1–Nse1(aa1–232)+6xHis-Nse3(aa1–328)+2xStrep-Nse4(aa1–300), pAW8–Nse3 (32) and pPM587-Nse3(aa1–328)+Nse4(aa1–300)+Nse1(aa1–232) plasmids. The sequences of primers used for mutagenesis are listed in Supplementary Table S3.

Expression and purification of human proteins

The pRP318 construct was used to express the full-length hNSE1/3 dimer in BL21(DE3)RIL *E. coli*. Transformed cells were incubated at 37°C to exponential phase (OD_{600} = 0.6–0.8) followed by 0.5 mM IPTG expression induction at 18°C overnight (16–18 h). The cell pellet was resuspended in lysis buffer (50 mM Na-phosphate, pH 7.4, 500 mM NaCl, 10% glycerol, 0.5 mM TCEP, 10 mM imidazole and 0.5% Triton X-100). The protein dimer was purified from the cell extracts using Talon metal affinity resin (Clontech). The 6xHis-tag was (optionally) cleaved off by addition of S-TEV protease, and then applied to a gel filtration column (Superdex 200 16/600, GE Healthcare). The resulting hNSE1/3 protein dimer was concentrated to 10–20 mg/ml in gel filtration buffer (50 mM Na-phosphate, pH 7.4, 500 mM NaCl, 5% glycerol and 0.5 mM TCEP) using Amicon Ultra-4 (UFC801024, Millipore), frozen in liquid N_2, and stored at −80°C until required.

The pRSFDuet-1–6xHis-hNSE1(aa1–266) and pET-28c–6xHis-hNSE3(aa1–304) constructs were used to transform BL21(DE3)RIL *E. coli*, and to prepare full-length recombinant 6xHis-hNSE1 and 6xHis-hNSE3 proteins, respectively. The expression and purification procedures were as described for the hNSE1/3 dimer (the S-TEV protease cleavage step was omitted).

To purify the human hNSE1-FL/hNSE3-FL/hNSE4b(aa92–212) (hNSE1/3/4) trimer, the KC808 construct was transformed into BL21(DE3)RIL *E. coli* cells. The cells were incubated at 37°C to exponential phase followed by 0.5 mM IPTG induction of expression at 16°C O/N. The protein sub-complex was purified from the cell extract using Talon metal affinity resin (Clontech). The 6xHis-tag and Strep-tag were subsequently cleaved off by addition of S-TEV protease. The cleaved sub-complex was separated from un-cleaved using a 5 ml heparin column (GE Healthcare) with an NaCl gradient elution step. Gel filtration chromatography (Superdex 200 16/600, GE Healthcare) was used as the last step of the purification. The resulting hNSE1/3/4 protein sub-complex was concentrated to 10–20 mg/ml in gel filtration buffer using Amicon Ultra-4, frozen in liquid N_2, and stored at −80°C until required.

Expression and purification of *S. pombe* trimer

The KC661 construct was used for expression of the *S. pombe* NSE1/3/4 trimer. The expression vector was transformed into BL21(DE3)RIL *E. coli*. The cells were grown in liquid non-inducing growth medium MDAG-11 (38) at 37°C overnight. The growth culture (OD_{600} = 5–7) was subsequently inoculated into auto-inducing medium ZYM5052 (38) (culture dilution 1:100) and grown at 16°C for 48 h (to OD_{600} = 20–30). The cell pellet was resuspended in lysis buffer. The protein sub-complex was purified from the cell extract using Talon metal affinity purification followed by Strep-tactin purification (IBA resins). The trimer was eluted from the resins by Strep-tactin elution buffer (50 mM Na-phosphate, pH 7.4, 300 mM NaCl, 5% glycerol and 0.5 mM TCEP and 2.5 mM D-desthiobiotin) and concentrated to 5–10 mg/ml using Amicon Ultra-4, frozen in liquid N_2, and stored at −80°C until required.

EMSA

Fluorescently labelled oligonucleotides were purchased from Sigma–Aldrich. The oligonucleotide sequences are listed in Supplementary Table S4 and Supplementary Figure S4D and E. The DNA substrates were prepared by annealing of 2–4 oligonucleotides (10 μM final concentration) in annealing buffer (50 mM Tris·HCl (pH 7.5), 100 mM NaCl and 10 mM $MgCl_2$). The oligonucleotide mixtures were boiled and slowly cooled down to room temperature. The quality of the DNA substrates was tested on native 7% or 20% (w/v) acrylamide (37.5:1 acrylamide:bisacrylamide) gels in 0.5× TBE buffer and stained with GelStar Nucleic Acid Gel Stain (Lonza).

Protein–DNA binding reactions were performed in 10 μl volumes containing a constant amount of fluorescently labelled DNA substrate (1 pmol) in each of the reactions and various concentrations of protein (0–24 pmol) in 50 mM sodium phosphate (pH 7.4), 50 mM NaCl (or 150 mM NaCl – only Figure 3 and Supplementary Figure S5B) and 0.1 mg/ml BSA. Reaction mixtures were incubated for 1 h on ice. Protein–DNA complexes were resolved on horizontal 4% (w/v) acrylamide (37.5:1 acrylamide:bisacrylamide) gels in 0.25× TBE buffer (Bio-Rad tray 25 × 15 cm, 300 ml of gel). The electrophoresis proceeded at 6 mA for 4 h at 4°C (tank: Sub-Cell GT Cell BIO-RAD; powerpack: OmniPAC, MIDi 300 V 700 mA 150 W – 110/230 V). Gels were scanned by a FLA 7000 imaging system (GE Healthcare). The intensity of both bands (free DNA and protein–DNA complex band) wasquantified using Multi Gauge V3.0 software. The ratio of protein–DNA to the total DNA was calculated to get percentage of bound DNA. Experimental data were plotted and fitted to a one-site specific binding model (with Hill-slope), using non-linear regression in Prism 6 (GraphPad Software, La Jolla, USA), in order to determine the reported disassociation constants (K_d).

Generation of *nse3* mutant strains of *S. pombe*

The *nse3* mutant strains were created using the Cre recombinase-mediated cassette exchange as described in our previous work (32). Briefly, *nse3*$^+$ flanked by loxP and loxM3 sites in pAW8 (*LEU2* marker) plasmid was mutated and transformed into the *nse3*$^+$*::ura4*$^+$ strain (Supplementary Table S5). *ura*$^+$, *leu*$^+$ transformants were selected in the presence of thiamine, grown in YES medium for 24 h, and then plated onto YES medium containing 5-fluoroorotic acid to select clones in which cassette exchange took place. 5-FOA^R and *leu*$^-$ colonies were picked and the presence of the expected mutations verified by sequencing. Strain crosses were carried out using standard genetic techniques (39). All the strains used in this paper are listed in Supplementary Table S5.

ade6-M216 nse3$^+$*::ura4*$^+$ strain was generated by crossing of *nse3*$^+$*::ura4*$^+$ strain with *ade6-M216* strain. Standard genetic techniques were used for preparation of diploid strain *nse3*$^+$*/nse3*$^+$*::ura4*$^+$ (39) crossing *ade6-M216 nse3*$^+$*::ura4*$^+$ strain with *ade6-M210*. The pAW8-Nse3-R261E construct was transformed into the *nse3*$^+$*/nse3*$^+$*::ura4*$^+$ diploid strain and the *nse3*$^+$*::ura4*$^+$ cassette was replaced as described in Hudson *et al.* (32), creating *nse3*$^+$*/nse3-R261E* diploid strain. Using standard genetic techniques (39), spores of the nse3$^+$/nse3-R261E strain were generated, dissected and analyzed.

Spot tests for sensitivity to DNA damaging agents

S. pombe cultures were grown to mid-log phase, concentrated to 3 × 10^7 cells/ml, and serial 10-fold dilutions were spotted onto rich media with indicated dose of DNA-damaging agent. Subsequently, plates were incubated at the indicated temperature (28 or 37°C) for 3–4 days.

Yeast hybrid assays

The Gal4-based Y2H system was used to analyze *S. pombe* Nse3 mutants. For five-component Y2H tests, three plasmids pGBKT7-Smc5(aa1–323+732–1065), pGADT7-Smc6(aa1–1140) and pPM587-Nse3+Nse1+Nse4 (LJ38) or its mutant versions were co-transformed into the *Saccharomyces cerevisiae* PJ69–4a strain and selected on SD -Leu, -Trp, -Ura plates. Drop tests were carried out on SD -Leu, -Trp, -Ura, -His (with 0, 1, 2, 5, 10 mM 3-aminotriazole) plates at 30°C. Each mutant was co-transformed at least twice into the yeast strain and at least two independent drop tests were carried out from each transformation.

Microscopy

For DNA and cell septa staining, exponentially growing *S. pombe* cells cultivated at 30°C in YES medium were harvested, incubated for 5 min in 75% ethanol, washed twice in PBS buffer, and then resuspended in water supplemented with DAPI at 1 μg/ml and Calcofluor at 20 μg/ml final concentrations. Microscopy was performed on Axio Imager Z1 microscope (Zeiss, Germany) with a 63×/1.4 oil objective lens. Images were captured on AxioCam MRm camera using Axio Version 4.8 software (Zeiss, Germany). Data are plotted as means ± standard deviation from triplicate counts of 200 cells.

ChIP

The *nse4-FLAG* strain MMP21 (40) was crossed with the *nse3-R254E*, *smc6-X*, or *smc6–74* strain. The untagged wild-type strain was used as a negative control in the ChIP assay. All cells were cultivated into mid-log phase. Then cells were either pretreated with 10 mM HU (4 h) or 0.005% MMS (5.5 h) or directly incubated with formaldehyde to cross-link DNA–protein complexes. Chromatin immunoprecipitation was performed using a protocol modified from Watson (41). Monoclonal anti-FLAG M2 antibody (Sigma; cat. num. 1804) was diluted 1:150, incubated with cell extract for 1 h on ice and precipitated with Dynabeads protein G (Invitrogen). After overnight incubation, several washes, elution and de-crosslinking, the DNA was purified using QIAquick PCR Purification Kit (Qiagen). The relative amount of PCR product was quantified by qPCR using SensiFAST^{TM} SYBR Hi-ROX Kit (Bioline). The sequences of primers used for the quantitative detection of the chromosomal loci were taken from (42). Input DNA recovery was calculated as: 2 squared [C_T(input) − C_T(immunoprecipitate)]. Melt curve analysis was performed for each sample after PCR amplification to ensure that a single product was obtained. The amount of the spNse4-FLAG protein in both input and immunoprecipitated samples was controlled by western blotting. For the protein detection on the membrane, monoclonal anti-FLAG M2-Peroxidase (HRP) antibody was used (Sigma, cat. num. A8592-1MG).

RESULTS

The human NSE3 protein binds to DNA

In our previous studies, we focused on the NSE3 protein and its protein–protein interactions with other subunits of the SMC5/6 complex (32,43,44). The human NSE3 (hNSE3) protein consists of two WH domains, WH-A and WH-B (PDB: 3NW0, (33,45)). The WH domain is a typical DNA-binding motif often positively charged at its DNA-binding surface, which is primarily formed by its third helix and wing (46,47). We have identified such a pattern within the C-terminal WH-B domain of the NSE3 subunit. This WH-B is folded into a putative DNA-binding conformation (Figure 1A) and contains at least three evolutionarily conserved positively charged residues within its third helix and wing (Figure 1B and Supplementary Figure S1B) suggesting its potential to bind DNA.

To test our *in silico* predictions experimentally, we expressed and purified full-length (FL) human NSE3 protein (hNSE3; Figure 1C). As yeast Smc5 and Smc6 proteins bind preferably to ∼50 nucleotide (nt) long ssDNA (26,27), we employed similar 45 nt ssDNA in our pilot electrophoretic mobility shift assay (EMSA) experiments (Figure 1D). Increasing concentrations of hNSE3 reduce the electrophoretic mobility of the 45 nt ssDNA substrate in the native gel, suggesting the formation of DNA–hNSE3 complexes (Figure 1D). This result suggests, consistent with our predictions, that hNSE3 protein binds DNA.

In contrast to hNSE3, two WH domains (N-terminal and C-terminal, WH-N and WH-C domains, respectively) of the human NSE1 (hNSE1) subunit were not predicted

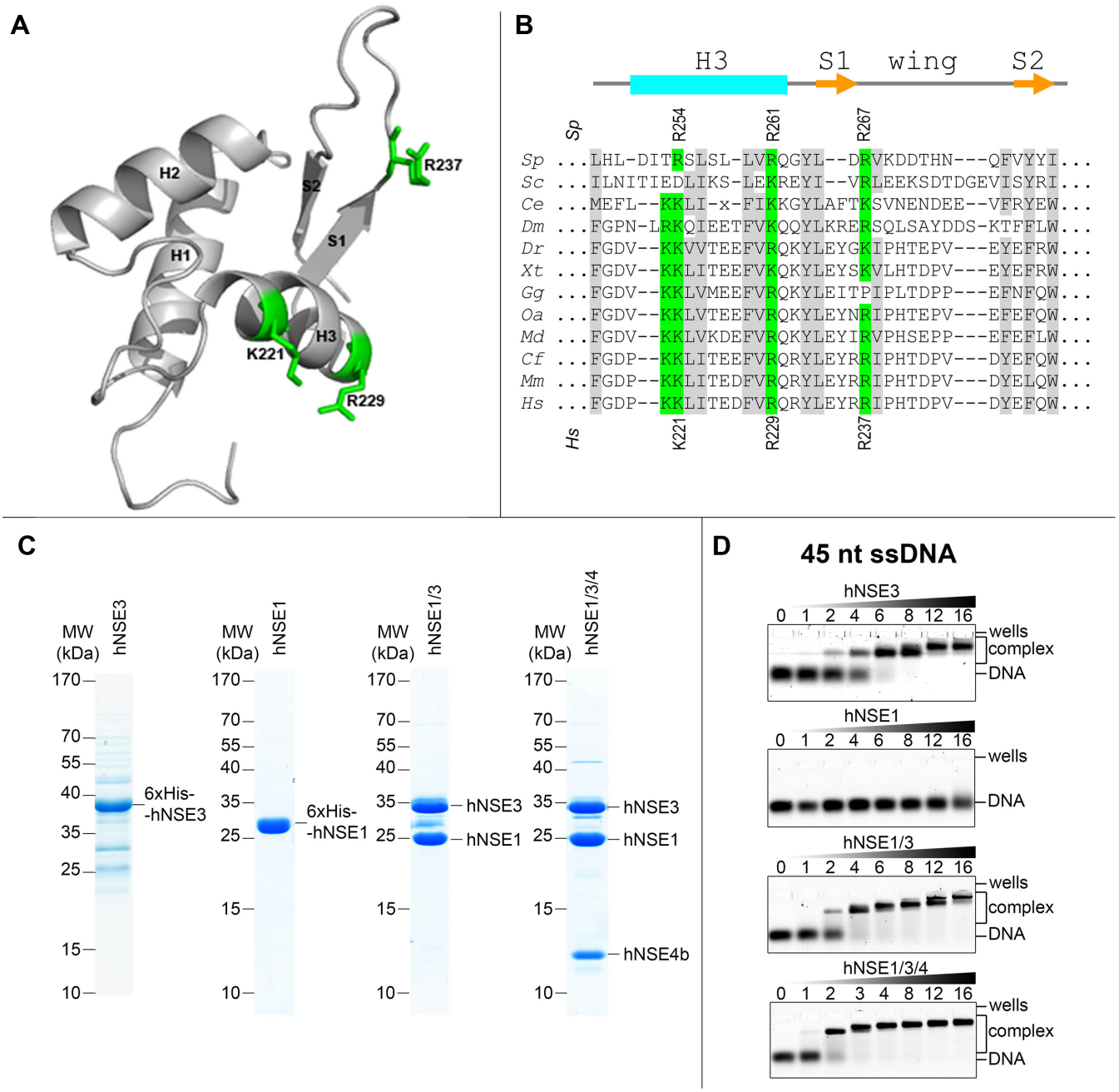

Figure 1. The human NSE3 protein binds DNA. (**A** and **B**) C-terminal part of NSE3 contains the putative DNA-binding winged helix B (WH-B) domain with conserved basic residues. (**A**) 3D structural model of the human NSE3 WH-B domain based on the crystal data (PDB: 3NW0). The WH-B domain is formed by helices H1–H3 and S1–wing–S2 region (S1, S2 – beta-sheets). (**B**) Alignment of the conserved helix H3 and S1–wing–S2 region sequences of NSE3 WH-B domain from different species: *S. pombe* (Sp), *S.cerevisiae* (Sc), *Caenorhabditis elegans* (Ce), *Drosophila melanogaster* (Dm), *Danio rerio* (Dr), *Xenopus tropicalis* (Xt), *Gallus gallus* (Gg), *Ornithorhynchus anatinus* (Oa), *Monodelphis domestica* (Md), *Canis lupus familiaris* (Cf), *Mus musculus* (Mm), *Homo sapiens sapiens* (Hs). Secondary structure of the WH-B domain corresponds to the structural model (**A**): cyan rectangle, helix; orange arrow, beta-sheet. Shading represents amino acid groups conserved across the family: hydrophobic, grey; basic, light green. Three most conserved basic residues within the DNA-binding motif are indicated (**A** and **B**). (**C**) Purified 6xHis-hNSE3-FL monomer (hNSE3), 6xHis-hNSE1-FL monomer (hNSE1), hNSE1-FL/hNSE3-FL dimer (hNSE1/3) and hNSE1-FL/hNSE3-FL/hNSE4b(aa92–212) trimer (hNSE1/3/4), respectively, were resolved by SDS-PAGE and stained with Coomassie blue dye. (**D**) EMSA. Fluorescein-labelled 45 nt ssDNA was mixed with increasing concentrations of indicated proteins and incubated on ice for 1 h. Reaction mixtures were analyzed on native 4% PAGE. While only free ssDNA-containing bands are visible after incubation with hNSE1, incubation of ssDNA with the other hNSE3-containing proteins results in slow-migrating bands suggesting the formation of DNA–protein complexes. The protein:DNA molar ratios (0, 1, 2, 4, 6, 8, 12, 16) are indicated at the top of each gel.

to have DNA-binding ability. The WH-N domain wing is buried in the hNSE1 structure (and therefore not available for DNA interaction; PDB: 3NW0) and the WH-C domain H3 helix and wing contain no conserved basic residues (Supplementary Figure S2). Consistent with these predictions, the purified full-length hNSE1 protein (Figure 1C) is not able to bind DNA in our EMSA experiments (Figure 1D).

As NSE3 protein exists within the NSE1/3/4 sub-complex in cells (29,31), we next purified the human NSE1/NSE3 (hNSE1/3) dimer, as previously reported (Figure 1C; (33)), and used it in EMSA experiments (Figure 1D). Interestingly, the hNSE1/3 dimer binds to the DNA substrate with slightly higher affinity than the hNSE3 monomer alone suggesting a putative role for hNSE1 in the binding of the dimer to DNA, but only in the presence of hNSE3 (Figure 1D; see below).

Our attempts to express and purify either full-length human NSE4b (hNSE4b) alone or whole hNSE1/hNSE3/hNSE4b trimer failed, but we successfully purified a human NSE1-FL/NSE3-FL/NSE4b(aa92–212) trimer (hNSE1/3/4), containing the hNSE1- and hNSE3-binding region of hNSE4b (32,43) (Figure 1C). The DNA-binding affinity of this hNSE1/3/4 trimer is comparable to that of the hNSE1/3 dimer (Figure 1D), suggesting that the hNSE3 subunit is the key DNA-binding subunit of this sub-complex.

The human NSE3 sub-complexes bind DNA without any preference for DNA-replication/recombination intermediates

To analyze the selectivity of the human NSE3 sub-complexes, we first compared their binding to ssDNA and dsDNA of different lengths. The hNSE1/3/4 trimer is not able to bind to 10 nt ssDNA and only slightly to 10 bp dsDNA (Figure 2A–D; Supplementary Figure S3A and S3B). In contrast, the longer 15 bp dsDNA substrate is efficiently bound ($K_d \sim 0.27$ μM), whilst the 15 nt ssDNA is only slightly shifted in our EMSA experiments, suggesting preferential binding of the hNSE1/3/4 trimer to short dsDNA (Figure 2A–D; Supplementary Figure S3A and S3B). The binding affinity of the trimer does not increase further with longer lengths of dsDNA (Figure 2B and D; Supplementary Figure S3B). However, the binding affinity of the trimer to ssDNA increases with the longer substrate lengths tested (Figure 2A and C; Supplementary Figure S3A). Levels of ssDNA–protein complexes are only comparable to the dsDNA–protein levels when 29 nt substrates are used (Supplementary Figure S3A and S3B). We note that the purified hNSE1/3 dimer has slightly lower affinity to the shorter (10 bp) dsDNA substrates than the hNSE1/3/4 trimer (Supplementary Figure S3B and S3D), suggesting that hNSE4b protein might also play a role in facilitating DNA-binding. Again, the dimer binds selectively to short dsDNA substrates while its affinity to both ssDNA and dsDNA substrates longer than 45 nt, is comparable (Supplementary Figure S3C and S3D).

As we used random sequence oligonucleotides for the above experiments we could not exclude the possibility that the long ssDNA substrates might fold to generate regions of double-stranded secondary structure. To avoid this possibility, we employed homopolymeric oligonucleotides (poly(dA) and poly(dT)) in EMSA experiments. The hNSE1/3/4 trimer exhibits little or no affinity for poly(dA) ssDNA (29 and 45 nts, respectively; Figure 2E and G), while binding to a duplex poly(dA)·poly(dT) (29 and 45 bp; $K_d \sim 0.2$ μM; Figure 2F and G) is comparable to the random sequence dsDNA of the same length ($K_d \sim 0.25$ μM; Figure 2B and D). Note, that hNSE1/3/4 appears to have low affinity for the 45 nt poly(dA) ssDNA substrate; the long homopolymeric oligonucleotide poly(dA) can still form secondary structures (48). Together, these data suggest a preference of the human NSE3 sub-complexes for dsDNA.

Several studies have suggested a role for the SMC5/6 complex in homologous recombination and replication fork stability (5,7,49,50). Therefore, we employed a panel of replication- and recombination-mimicking DNA molecules and tested them against the hNSE1/3/4 trimer (as well as the human dimer) (Figure 2H; Supplementary Figure S4). Surprisingly, we observed no significant difference in DNA-binding affinity of the human NSE3 sub-complexes to either of the specific DNA substrates in comparison to the 45 bp dsDNA (Figure 2; Supplementary Figure S4), suggesting that the human NSE3 sub-complexes bind to dsDNA without any preference for DNA-replication/recombination intermediates.

Several subdomains of human hNSE1/hNSE3/hNSE4b trimer mediate its binding to DNA

Our *in silico* analysis identified several conserved basic residues within the helix H3 and wing of the WH-B domain of NSE3 (Figures 1 and 3A – left). To test their role in the NSE3–DNA interaction, we first mutated arginine 229 of hNSE3 to glutamic acid. We purified the R229E mutant version of the hNSE1/3/4 trimer (Supplementary Figure S5A) and compared its binding affinity to a 21 bp dsDNA with the wild-type (WT) trimer (Figure 3B and C). The R229E mutation significantly reduced the binding affinity of the trimer to the dsDNA substrate. Mutations of similarly conserved amino acids Lys221 (K221E) and Arg237 (R237E) in the hNSE3 WH-B domain, like the R229E mutant, decreased the affinity of the trimer for dsDNA, thereby suggesting an important role for the WH-B domain of hNSE3 in DNA binding.

The reported X-ray crystal structure of the human NSE1/3 dimer (PDB: 3NW0) shows that the hNSE3 WH-B subdomain, together with a positively charged hNSE1 loop (comprised of amino acids 139–144) forms a distinct cleft or channel (Figure 3A – left, green-labelled residues; Supplementary Figure S2B), which is interesting, as our EMSA results suggest a role for hNSE1 in promoting the efficient binding of the hNSE1/3 dimer to DNA (Figure 1D). To test whether the hNSE1/3/4 trimer binds DNA through the basic residues found in this cleft, we introduced the mutation K139E into the hNSE1 loop (Figure 3B and Supplementary Figure S2B and S5). Pleasingly, the mutant hNSE1-K139E has significantly lower affinity to dsDNA than the wild-type trimer (Figure 3B and C). The double mutant hNSE1-K139E/hNSE3-R229E trimer has even lower affinity to DNA than either of the single hNSE1-K139E or hNSE3-

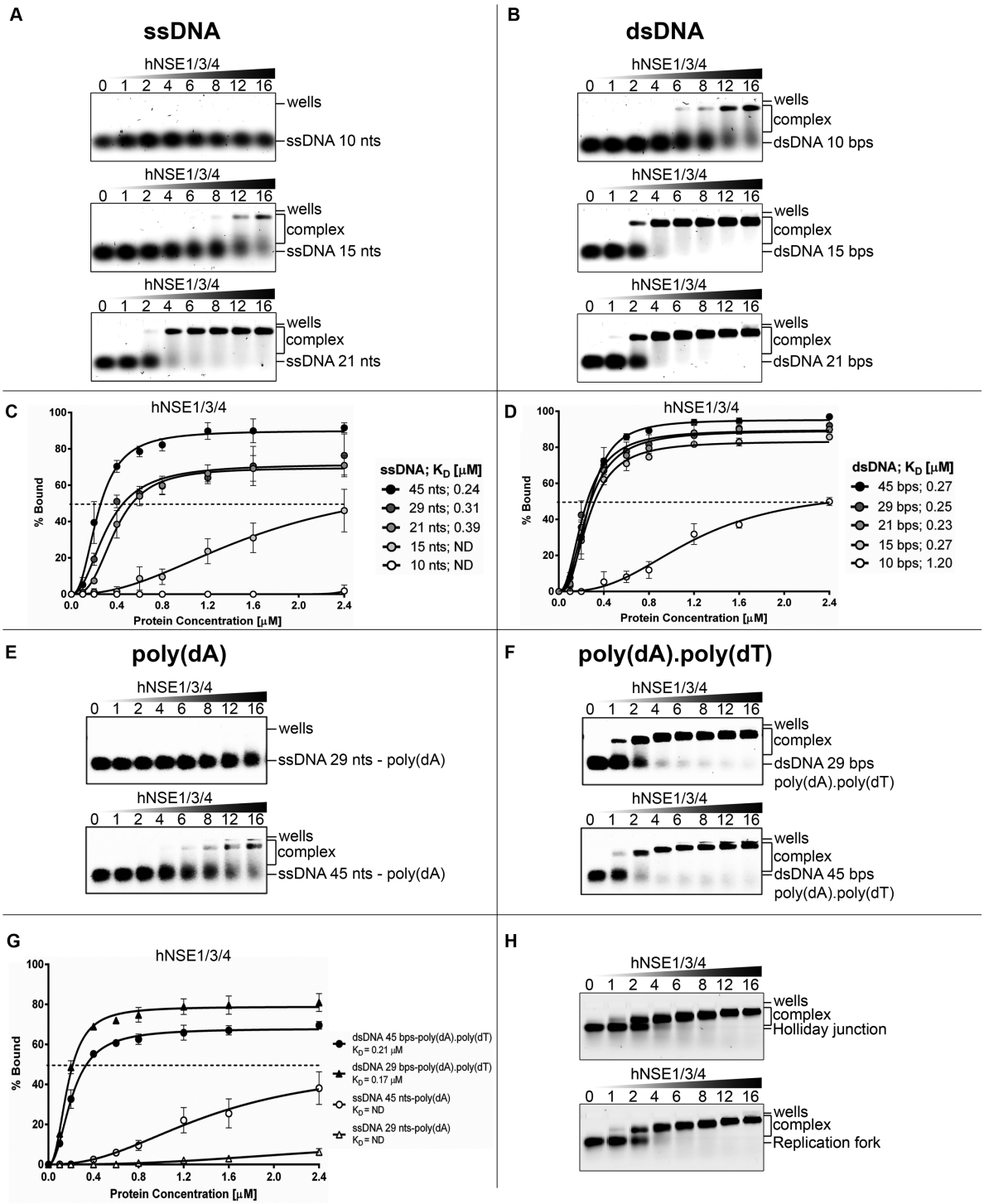

Figure 2. The hNSE1/3/4 trimer binds to dsDNA without any preference for DNA-replication/recombination intermediates. Reaction mixtures containing 10, 15, 21, 29 or 45 nt ssDNA with random sequence (rs) (**A**, **C**), 10, 15, 21, 29 or 45 bp dsDNA-rs (**B**, **D**), 29 or 45 nt ssDNA poly(dA) chain (**E**, **G**), 29 or 45 bp dsDNA with annealed poly(dA)·poly(dT) chains (**F**, **G**), and Holliday junction or replication fork substrates (**H**) were incubated with increasing concentrations of hNSE1/3/4. The hNSE1/3/4–DNA complexes were analyzed using EMSA (further details as in Figure 1D). The 15 bp dsDNA-rs (**B**) is efficiently bound by hNSE1/3/4, while the 15 nt ssDNA-rs (**A**) is not. Both 21 nt ssDNA and dsDNA substrates with random sequences are shifted in the presence of the hNSE1/3/4 trimer (**A**–**D**), although the ssDNA substrate is bound with lower affinity than the dsDNA. The poly(dA) ssDNA substrates (**E**, **G**), which form fewer secondary structures or homodimers than random sequence ssDNA**,** are not or just slightly shifted in EMSA. In contrast, hNSE1/3/4 has similar affinity to both 29 or 45 bp poly(dA).poly(dT) dsDNA (**F**, **G**) as to the 29 or 45 bp dsDNA-rs (**D**). (**C**, **D**, **G**) Quantification of EMSA results in the graphs with standard deviation and calculated K_d is based on at least three independent experiments (threshold level for K_d calculations is labelled by dashed line; more examples are shown in Supplementary Figure S3). (**H**) The EMSA experiment with the human NSE1/3/4 sub-complex and Holliday junction or replication fork DNA substrates. The hNSE1/3/4 trimer has similar affinity to these structures as to dsDNA (15–45 bp). Therefore, hNSE1/3/4 has no selective binding to recombination/replication-mimicking substrates *in vitro* (more examples are shown in Supplementary Figure S4).

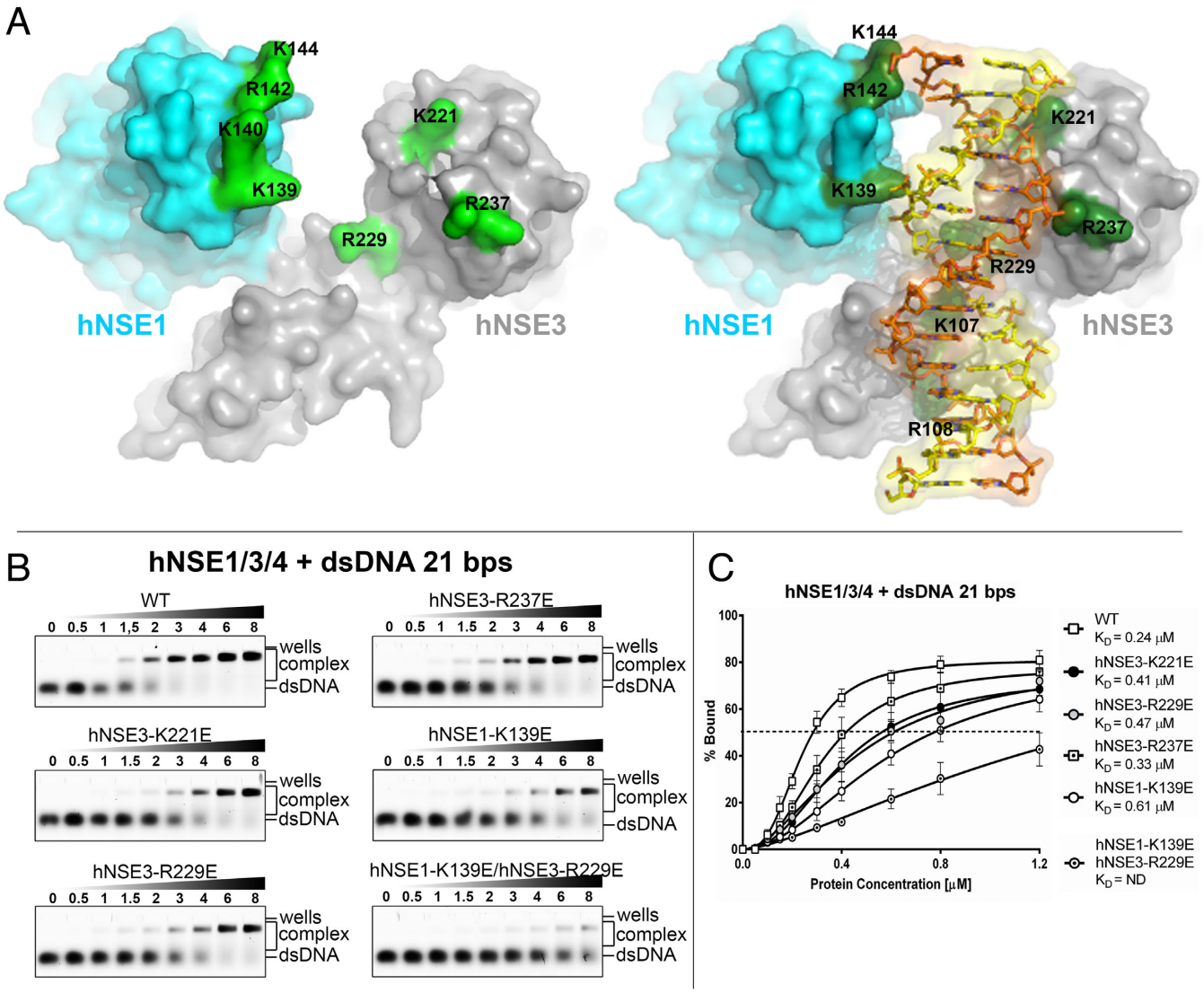

Figure 3. The human NSE1/3/4 trimer binds DNA through its cleft formed by the hNSE3 WH-B domain and the hNSE1 loop. (**A**) (Left) Molecular surface representation of the human NSE1/3 sub-complex (PDB: 3NW0) coloured to highlight basic residues (light green) of the putative DNA-binding cleft, which is formed by the hNSE3 (gray) WH-B domain and the hNSE1 (cyan) loop. (Right) Representative docking pose of NSE1/3 in complex with a 15 bp B-form DNA duplex. Basic residues in proximity to the DNA-duplex are coloured in dark green. The docked DNA is shown in a combined surface/stick surface representation (coloured yellow/orange). (**B**) The binding affinity of purified trimers to 21 bp dsDNA was analyzed using EMSA buffer with 150 mM NaCl (further details as in Figure 1D). (**C**) Quantification of EMSA results in the graphs with standard deviation and calculated K_d is based on at least three independent experiments.

R229E mutant trimers (Figure 3B and C). These data indicate that both the hNSE3 WH-B domain and the hNSE1 loop, which together form the cleft, are both involved in binding to DNA.

To integrate our *in silico* (Figure 3A – left) and experimental data (Figure 3B), we docked a B-form DNA duplex into the human NSE1/3 crystal structure (PDB: 3NW0). Figure 3A (right) shows that the duplex is readily accommodated by the proposed DNA-binding cleft and that the basic residues important for DNA-binding are poised to make sequence non-specific interactions with the sugar-phosphate backbone (hNSE1 – K139 and hNSE3 – K221, R229, K237E). To prove the model, we additionally introduced glutamic acid mutations of hNSE1 Arg142 and Lys144 (hNSE1-R142E+K144E) into the human trimer (Supplementary Figure S5A). Consistent with our model, the hNSE1-R142E+K144E mutant trimer shows a similar reduction of affinity to dsDNA to that of hNSE1-K139E single mutant trimer (Supplementary Figure S5B and S5C). Furthermore, our docked model also places the dsDNA sugar-phosphate backbone in close proximity to WH-A evolutionarily conserved hNSE3 K107 and R108 residues (Figure 3A – right and Supplementary Figure S1A). Therefore, we finally created hNSE3-K107E+R108E (Supplementary Figure S5A) and tested its ability to interact with dsDNA. Indeed, the hNSE3-K107E+R108E double mutation significantly reduced the dsDNA binding affinity of the trimer (Supplementary Figure S5B and S5C). Altogether, our EMSA results and model suggests that both WH-A and

WH-B domains of NSE3 and the NSE1 loop (aa139–144) bind to dsDNA.

Note that the affinity of wild type hNSE1/3/4 to dsDNA ($K_d \sim 2 \times 10^{-7}$M; Figure 3C) is lower than typical sequence specific DNA-binding proteins ($K_d = 10^{-13}$–10^{-9} M). Therefore, our docking model together with the determined K_d value for the affinity of the trimer for dsDNA are consistent with previous data indicating a sequence non-specific binding mode of the SMC5/6 complex to DNA (42).

The NSE3–DNA interaction is evolutionarily conserved from yeast to human

To test if the NSE1/3/4–DNA interaction is evolutionarily conserved (Figure 1B), we next attempted to prepare recombinant *S. pombe* Nse1, Nse3 and Nse4 proteins. On its own, the Nse3 monomer was insoluble in *E. coli*, however expression of the *S. pombe* Nse1/Nse3/Nse4 (spNSE1/3/4) trimer produced a soluble complex, which we were able to purify to ∼85% purity (Figure 5A). In EMSA experiments, the spNSE1/3/4 trimer behaved similarly to the human NSE3 sub-complexes, albeit with lower DNA-binding affinity ($K_d \sim 1$ μM; Figure 4). As observed with the human NSE3 sub-complexes, the spNSE1/3/4 trimer binds preferentially to short dsDNA over ssDNA (Figure 4A–D). For complete binding of the *S. pombe* trimer, the length of the dsDNA must be greater than 29 bps and the affinity of the trimer is not increased with longer dsDNA substrates over 45 bp (K.Z., unpublished data). The preferential binding to dsDNA (over ssDNA) is clearly visible when poly(dA) ssDNA is compared with poly(dA)·poly(dT) dsDNA (Figure 4E and F). In addition, no increased affinity to the replication- and recombination-mimicking DNA substrates is observed (Supplementary Figure S6).

Secondly, to test our hypothesis that the NSE3–DNA interaction is mediated by the evolutionarily conserved WH-B domain (Figure 1A and B), we mutated key basic residues (Arg254 and Arg261) of *S. pombe* Nse3 to glutamic acid (which correspond to K221E and R229E mutations in the human NSE3 WH-B domain). The mutant spNSE1/3/4 trimers were purified to the same extent as the WT complex (Figure 5A), with the same stoichiometric ratio of 1:1:1, and then used for our EMSA experiments (Figure 5B). The introduced mutations had no visible effect on the integrity of either the purified spNSE1/3/4 sub-complex or the intact SMC5/6 complex in 5-component Y2H (Figure 5A and D), suggesting no defect of SMC5/6 protein–protein interactions (although the definitive conclusions about the stability of SMC5/6 will require *in vivo* co-immunoprecipitation from yeast cells). In contrast, both mutations severely disturbed DNA-protein interactions of spNSE1/3/4. Both the Nse3-R254E and Nse3-R261E mutant spNSE1/3/4 complexes exhibited very low affinity to 45 bp dsDNA (Figure 5B and C). In addition, we also changed Arg261 of the Nse3 subunit to glutamine (Figure 5A). While the glutamic acid mutation changes the positive charge of arginine to negative, the glutamine mutation of arginine just abolishes its positive charge. Indeed, the R261Q mutant of the spNSE1/3/4 trimer had lower affinity to dsDNA than wild type, but it had higher affinity to dsDNA than the R261E mutant (Figure 5B and C). Together, these results suggest that the interaction of the NSE1/3/4 sub-complex with dsDNA, mediated through the NSE3 WH-B domain, is evolutionarily conserved.

The Nse3–DNA interaction is essential in fission yeast

To explore the function of the Nse3–DNA interaction in fission yeast, we introduced the above Nse3 protein mutations (R254E, R261E and R261Q) into the *S. pombe* genome. The integration of the *nse3-R254E* mutation results in a phenotype similar to that of *smc6–74* and *smc6-X* mutants (Figure 6A and B). The *nse3-R254E* mutant cells have decreased viability (Figure 6B and C) which is accompanied by higher levels of cells with diffuse fragmented DNA (2.6%) or misplaced nuclei (1.5%) and cells with mitotic abnormalities (2.5%) such as multiple septa, aneuploidy or 'cut' cells (Figure 6B and C). Interestingly, we were unable to isolate *nse3-R261E* mutant haploid cells and our tetrad analysis of the heterozygous *nse3*$^{+}$/*nse3-R261E* diploid strain suggested that this mutation is lethal (Figure 6D). In contrast to *nse3-R261E*, the *nse3-R261Q* mutant cells show higher viability than *nse3-R254E* (Figure 6A and B). The mild *nse3-R261Q* phenotype versus severe phenotype of *nse3-R254E* (and lethal phenotype of *nse3-R261E*) are in good agreement with our EMSA results as the Nse3-R261Q protein has significantly higher affinity to dsDNA than Nse3-R254E and Nse3-R261E proteins (Figure 5B and C). Altogether, the severe or lethal phenotypes of *nse3-R254E* and *nse3-R261E* suggest general problems in chromatin maintenance and an essential role of Nse3–DNA binding activity for the SMC5/6 complex in yeast.

Similar to other *smc5/6* hypomorphic mutants (e.g. *smc6-X* and *smc6–74*), the *nse3-R254E* mutant exhibits hypersensitivity to hydroxyurea (HU), which induces replication stress, and to DNA-damaging agents, e.g. methyl methanesulfonate (MMS), UV light and others (Figure 6A) indicating problems with replication and DNA-repair processes. Furthermore, epistasis analysis of *nse3-R254E rad51Δ* double mutant suggests defects in HR repair (Figure 6E). The combination of *nse3-R254E* with an *rqh1* helicase deletion mutant is synthetically lethal (Figure 6F), suggesting defects in resolution of HR intermediates in our *nse3* hypomorphic mutant (40,51). Similarly, *nse3-R254E* is synthetically lethal in combination with a *brc1Δ* mutant (Figure 6F), suggesting a role of the Nse3–DNA interaction in stabilization of stalled replication forks (52). Consistent with this, the *nse3-R261Q* mutant exhibits a selective HU-sensitive phenotype (Figure 6A).

Association of the SMC5/6 complex with chromatin is dependent on the Nse3–DNA interaction in *S. pombe*

To analyze the role of the Nse3–DNA interaction in the accumulation of the SMC5/6 complex on chromatin, we attempted to tag *nse3* mutants or cross the *nse3-R254E* cells with *nse4*- or *smc6*-tagged *S. pombe* strains (42). Unfortunately, most of these tag combinations and crosses were lethal or had severe phenotypes (data not shown). Only the *nse3-R254E* mutant cells carrying *nse4-FLAG* allele (40) were viable and exhibited the same phenotype as the

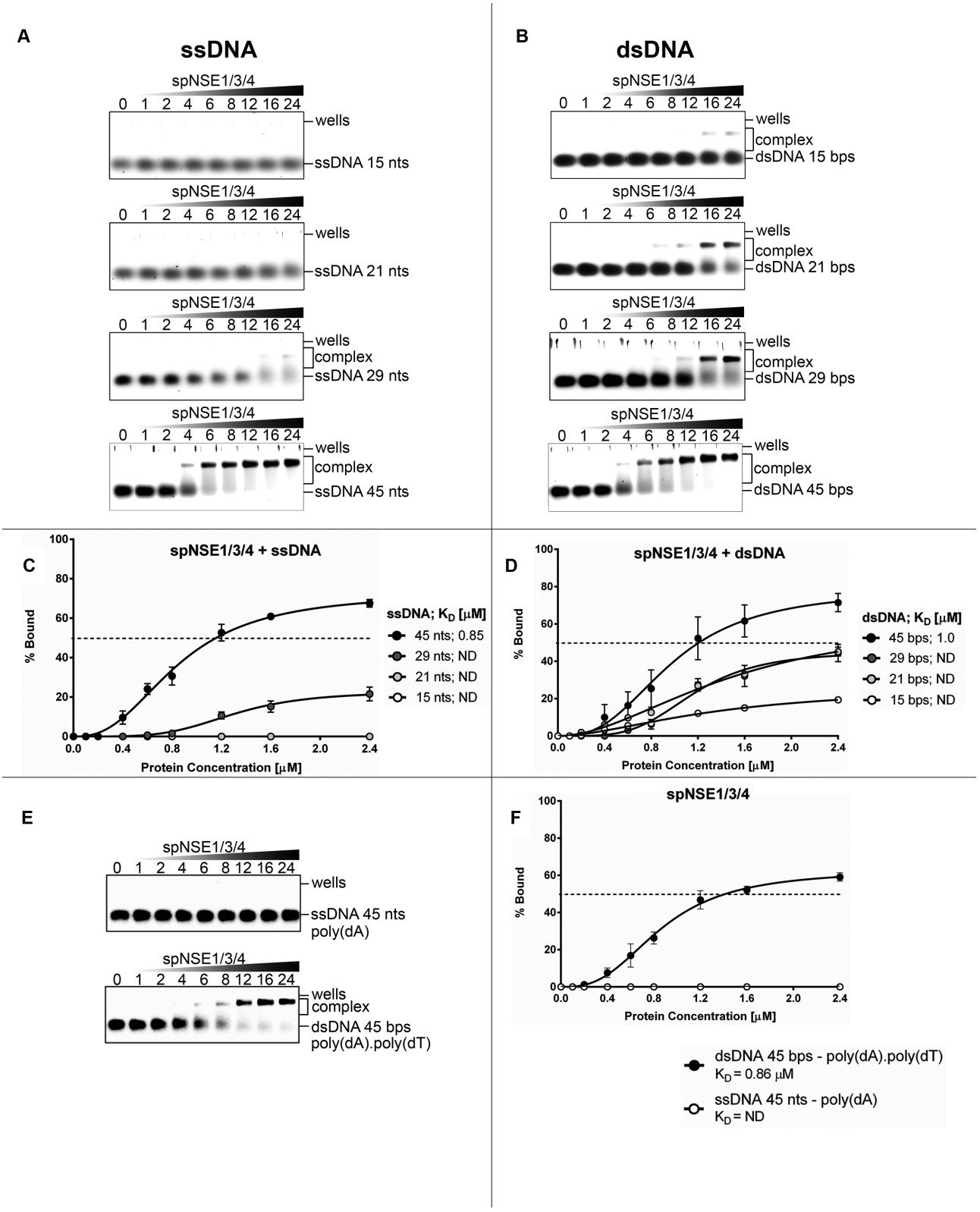

Figure 4. *S. pombe* NSE1/3/4 binds to dsDNA. Fluorescein-labelled 15, 21, 29 or 45 nt ssDNA (**A**, **C**) or dsDNA (**B**, **D**), or 45 nt poly(dA) ssDNA or 45 bp poly(dA).poly(dT) dsDNA (**E**, **F**) was mixed with increasing concentrations of spNSE1/3/4 (**A–F**) (further details in Figure 1D). (**C**, **D**, **F**) Quantification of EMSA results (based on at least three independent experiments with standard deviations and calculated K_d).

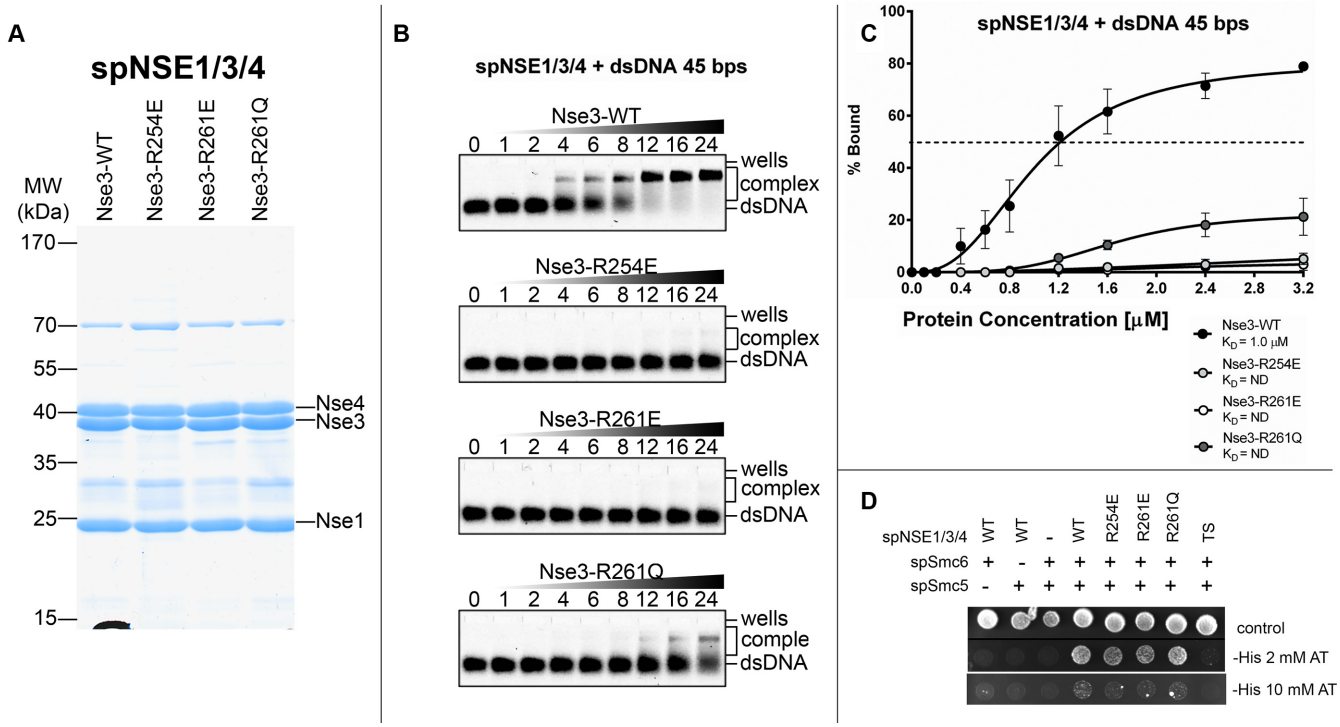

Figure 5. The yeast spNSE1/3/4 sub-complex binds dsDNA via its Nse3 WH-B domain. (**A**) Purified wild-type and mutant versions of the spNSE1/3/4 trimer were resolved by SDS-PAGE and stained with Coomassie Blue: *S. pombe* Nse1-WT/Nse3-WT/Nse4-WT (Nse3-WT), Nse1-WT/Nse3-R254E/Nse4-WT (Nse3-R254E), Nse1-WT/Nse3-R261E/Nse4-WT (Nse3-R261E) and Nse1-WT/Nse3-R261Q/Nse4-WT (Nse3-R261Q). (**B**, **C**) The binding affinity of the purified sub-complexes to 45 bp dsDNA was analyzed using EMSA (further details as in Figure 1D). (**C**) Quantification of EMSA results (based on at least three independent experiments with standard deviations and calculated K_d). (**D**) Stability of the yeast SMC5/6 complex was analyzed using five-component version of the Y2H system. SMC5 head domain (fused to Gal4/BD domain) and full-length SMC6 (fused to Gal4/AD domain) core subunits were co-transformed together with construct coding components of Nse1/3/4 (pPM587-Nse3+Nse1+Nse4). Growth of the transformants was verified on plates without Leu, Trp and Ura (control). Stability of the SMC5/6 complex was scored by growth of yeast transformants on plates without Leu, Trp, Ura and His, while containing 2 and 10 mM 3-Amino-1,2,4-triazole (-His +2 mM AT and -His +10 mM AT panels, respectively). The SMC5/6 complexes containing Nse3-WT (WT), Nse3-R254E (R254E), Nse3-R261E (R261E) and Nse3-R261Q (R261Q) mutations exhibited similar stability, while complex containing Nse3-Y264/L265A (TS) mutation was not stable. Note, stability of the Nse3 protein is compromised by the Y264/L265A double mutation (more details in (32)). In control experiments, either of the constructs was replaced with empty vector (−).

parental *nse3-R254E* mutant strain (Supplementary Figure S7A). Using FLAG-tag based ChIP–qPCR assay, we followed the FLAG-tagged Nse4 protein (spNse4-FLAG) chromatin localization in WT, *nse3-R254E*, *smc6–74* and *smc6-X* cells under normal growth conditions. Similar to previously reported results using *nse4-HA* (42), we observed enrichment of spNse4-FLAG at centromeric loci (central core domain *cnt2* and *dg2* repeats), *tRNA:Leu1,* ribosomal (*rDNA*) and subtelomeric (*Telo2R*) loci in WT cells (Figure 7A). Despite the severe phenotypes of the *smc6-X* mutant strain (Figure 6) (5), its spNse4-FLAG accumulation was similar to that in wild-type cells. In contrast, the accumulation of spNse4-FLAG protein was significantly reduced in the *nse3-R254E* mutant cells at all tested chromatin loci (Figure 7A), although the spNse4-FLAG expression level and the amount of the precipitated spNse4-FLAG protein was comparable in all strains (Supplementary Figure S7B). Interestingly, we observed a similar defect for spNse4-FLAG chromatin association in *smc6–74* mutant cells (Figure 7A), suggesting that both Nse3 binding to DNA and SMC6 ATPase activity is important for either SMC5/6 chromatin loading or its stable association with chromosomal loci in yeast.

As the SMC5/6 complex is involved in DNA repair and restart of stalled replication forks (Figure 6), we therefore followed spNse4-FLAG chromatin localization in WT and *nse3-R254E* after HU or MMS treatment. In the WT cells, the enrichment of spNse4-FLAG after HU treatment was similar to accumulation under normal conditions (Supplementary Figure S8). In the *nse3-R254E* mutant cells, accumulation of the spNse4-FLAG protein was significantly reduced similar to the levels seen under normal conditions. The MMS treatment resulted in reduced spNse4-FLAG levels at most loci in WT cells consistent with previous data (42). In the *nse3-R254E* mutant cells treated with MMS, spNse4-FLAG enrichment was again significantly reduced at most loci compared to untreated as well as MMS treated WT cells (Supplementary Figure S8), consistent with the above proposed general role of the Nse3–DNA interaction in either SMC5/6 chromatin loading or stable association of the SMC5/6 complex with chromosomal loci.

DISCUSSION

In this paper, we have described a novel DNA-binding mode of the SMC5/6 complex through the NSE1/3/4 subcomplex. The NSE1/3/4–DNA interaction is mediated by

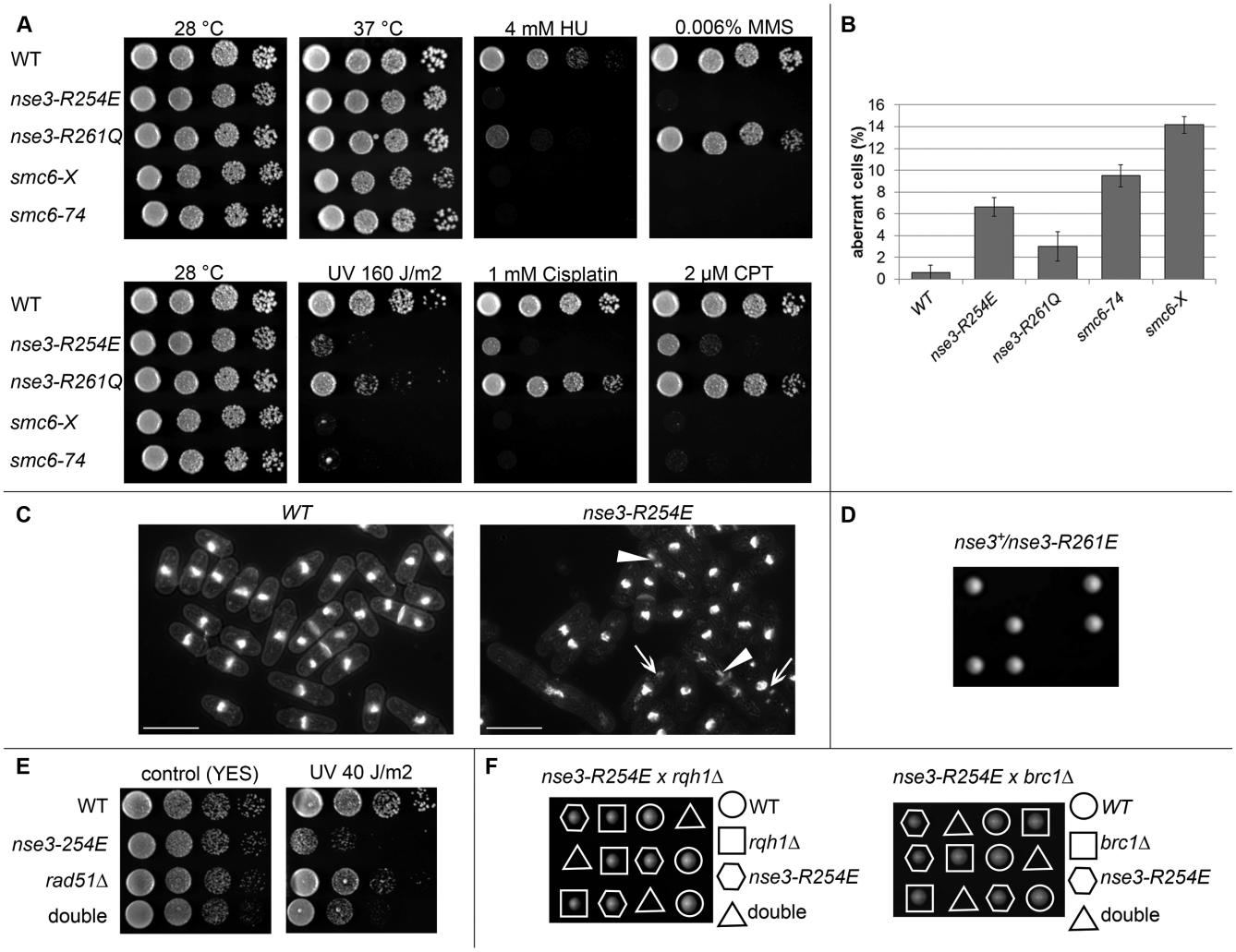

Figure 6. Mutations in the Nse3 DNA-binding motif result in chromatin aberrations and increased sensitivity to DNA damaging agents of the *S. pombe* cells. (**A**) The *S. pombe* Nse3 WH-B domain mutant strains (*nse3-R254E* and *nse3-R261Q*), and *smc6* hypomorphic mutants (*smc6-X* and *smc6–74*) were tested for sensitivity to DNA damaging agents. Tenfold serial dilutions of the indicated strains were plated onto media containing the following drugs: the dNTP depleter HU, the topoisomerase I poison camptothecin (CPT), Cis-platinum causing cross-linking of DNA and the alkylating agent MMS; or the plates were UV exposed. (**B**) The graph quantifies aberrant cells: diffuse fragmented DNA, no or misplaced nuclei and cells with mitotic abnormalities (multiple septa, aneuploidy, 'cut' phenotype). Data are means ± standard deviations from at least triplicate counts of 200 DAPI and calcofluor stained cells. (**C**) Examples of DAPI and calcofluor images of *WT* and *nse3-R254E* cells grown to mid-logarithmic phase at 30°C. Aberrant phenotypes: arrow – fragmented DNA, arrowhead – aberrant mitosis; bar – 10 µm. (**D**) Tetrad dissection analysis of yeast diploid strain *nse3*$^{+}$/*nse3-R261E*. *nse3-R261E* single mutation is lethal, suggesting essential role for the Nse3–DNA interaction in fission yeast. (**E**) *nse3-R254E* mutant is epistatic with *rad51*Δ. Double: mutant *nse3-R254E rad51*Δ. (**F**) Tetrad dissection analysis of yeast diploid strain *nse3-R254E*/*rqh1*Δ (left) and nse3-R254E/*brc1*Δ (right). *nse3-R254E rqh1*Δ and *nse3-R254E brc1*Δ double mutants are dead. Double: mutant *nse3-R254E rqh1*Δ (left panel) and *nse3-R254E brc1*Δ (right panel).

the WH-B domain of the NSE3 subunit, via highly conserved basic residues within helix H3 (Figures 1, 3 and 5). However, other parts of the NSE1/3/4 sub-complex also appear to contribute to DNA binding. Both experimental data and modelling indicate that the WH-A domain of NSE3 also participates in the interaction (Figure 3 and Supplementary Figure S5). Similarly, NSE1 can also interact with DNA, which is consistent with the composite surface formed by NSE1 when paired with NSE3 (Figure 3 and Supplementary Figure S5). NSE4 may also be involved in DNA interactions (directly or indirectly) potentially through a conformational change or stabilization of the NSE1/3/4 sub-complex (Figure 1).

NSE1/3/4 preferentially binds to dsDNA over ssDNA when short but not when long oligonucleotides are used (Figure 2 and 4, Supplementary Figure S3). NSE1/3/4 exhibits no preference for recombination- or replication-mimicking substrates (Supplementary Figures S4 and S6), suggesting that the NSE3–DNA interaction is primary involved in a general function of the SMC5/6 complex rather than in the repair function, which is not essential for cell division. Consistent with this, complete disruption of the DNA-binding ability of the spNSE1/3/4 sub-complex by the *nse3-R261E* mutation is lethal in fission yeast (Figure 6D), similar to the complete deletion of *nse3* gene (or any of the evolutionarily conserved subunits of SMC5/6) (5,28,53,54). We note that the Nse3-R261E mu-

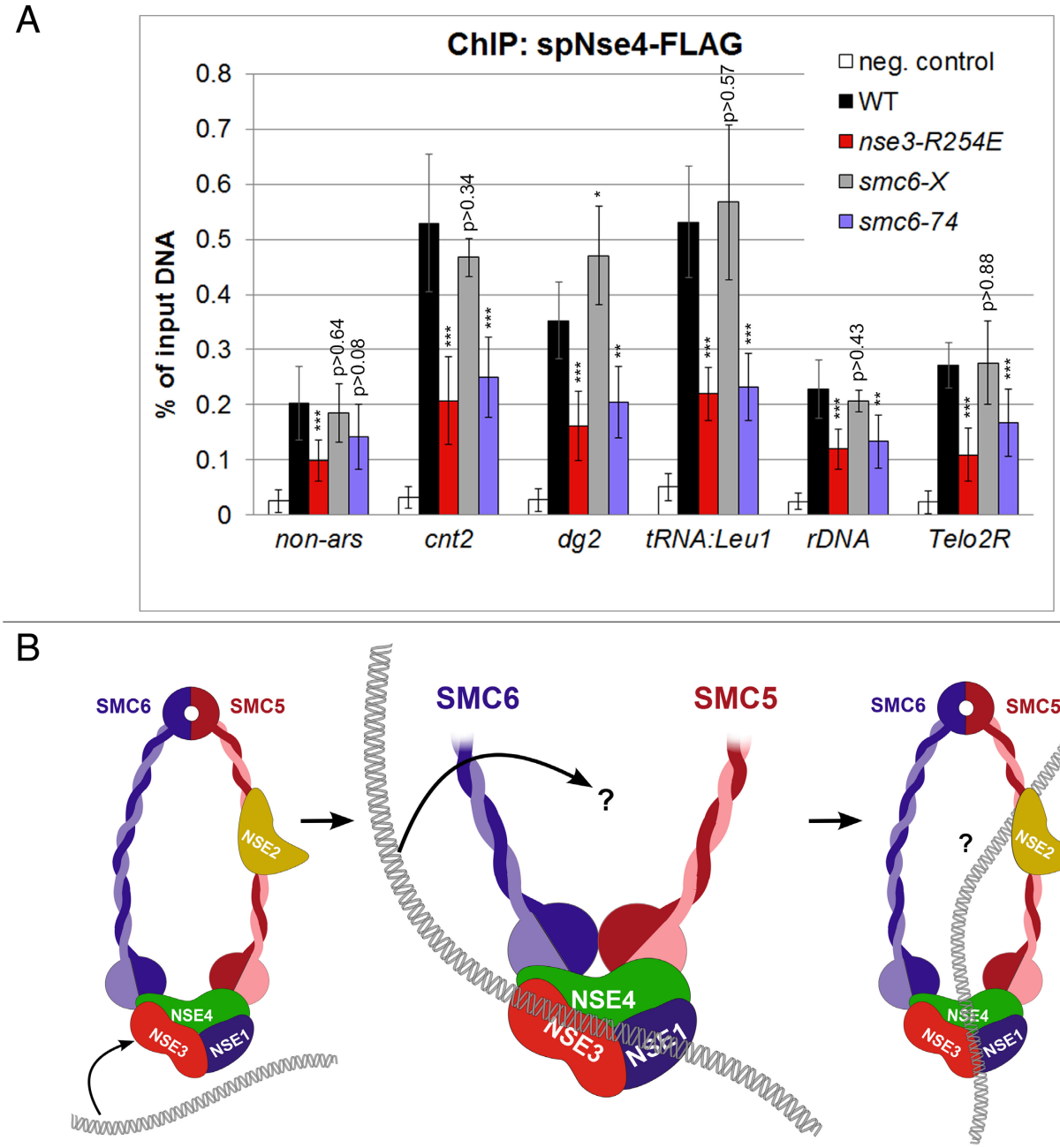

Figure 7. Association of the *S. pombe* SMC5/6 complex with chromatin is dependent on binding of the Nse3 WH-B domain to DNA. (**A**) Results of chromatin immunoprecipitation followed by quantitative PCR (ChIP–qPCR). Liquid cultures of *503* (neg. control), *nse4-FLAG nse3*$^{+}$ (WT), *nse4-FLAG nse3-R254E* (*nse3-R254E*), *nse4-FLAG smc6-X* (*smc6-X*) and *nse4-FLAG smc6–74* (*smc6–74*) yeast strains were grown in YES medium at 30°C to mid-log phase. Yeast extracts were made and immunoprecipitated using the anti-FLAG antibody. DNA which co-precipitated with the spNse4-FLAG protein was then analyzed using qPCR. The precipitated samples were compared with the total amount of DNA in the input samples (mean ± standard deviation, n ≥4 biological replicas). Actual p-value is indicated when >0.05, otherwise *P*-value <0.05 is indicated by *; <0.01 by **; and <0.001 by *** (*t*-test). (**B**) Hypothetical model for loading of the SMC5/6 complex onto chromatin. The NSE1/3/4 sub-complex binds dsDNA fiber (left), which may properly align DNA next to the SMC5/SMC6 ring (middle) or may induce conformational changes of the SMC5/6 complex and result in entrapment of the chromatin fiber inside the SMC5/6 ring (right).

tation influences neither the stability of the *in vitro* purified spNSE1/3/4 sub-complex (Figure 5A) nor its ability to bridge the Smc5-Smc6 heterodimer (Figure 5D; (29)). We therefore suggest that the NSE3–DNA interaction is essential for SMC5/6 function.

The *nse3-R254*E mutant strain, which has similar deficiency in DNA-binding capability to *nse3-R261E in vitro* (Figure 5B and C), has a reduced viability comparable to the *smc6–74* mutant and hypersensitivity to DNA-damaging agents similar to both *smc6-X* and *smc6–74* mutants (Figure 6). Both *smc6* hypomorphic mutants and *nse3-R254E* are implicated in HR (Figure 6E and F) (5,55). As homologous recombination is not essential for cell division in *S. pombe* and the NSE1/3/4 sub-complexes (neither yeast nor human) do not bind specifically to recombination-mimicking substrates *in vitro* (Supplementary Figures S4 and S6), we surmise that NSE1/3/4–DNA binding is not directly involved in the processing of HR intermediates. Similarly, NSE1/3/4 does not directly bind to replication-mimicking substrates *in vitro* (Supplementary Figures S4 and S6), although the *nse3-R254E* phenotype (Figure 6A and F) and *nse3-R261Q* specific HU sensitivity (Figure 6A) suggest a role of NSE3–DNA binding in stabilization or processing of stalled replication forks (7). It may also indicate an indirect role of NSE1/3/4 in stabilization and processing (via HR) of stalled replication forks through maintenance of chromatin structure (7,8).

Although the essential function of the SMC5/6 complex and how it is involved in maintenance of chromosomal structures is still not clear, its association with chromatin is a prerequisite for its full function. Interestingly, *nse3-R254E* and *smc6–74* (A151T) mutations significantly reduce the spNse4-FLAG protein binding at all tested chromosomal loci in comparison to wild-type cells in a ChIP assay (Figure 7A). In contrast, binding of the spNse4-FLAG protein in the *smc6-X* (R706C) mutant is similar to that observed in wild-type cells (Figure 7A). However, the sensitivity to DNA-damaging agents of *smc6-X* is comparable to *nse3-R254E* and *smc6–74* and the percentage of aberrant cells in the *smc6-X* culture is even higher than in *nse3-R254E* and *smc6–74* (Figure 6). These data suggest that the *nse3-R254E* and *smc6–74* mutants, but not *smc6-X*, could be defective in loading onto chromatin, in stable binding or accumulation of the SMC5/6 complex at specific chromatin loci.

Although we analyzed only selected chromosomal loci, the spNse4-FLAG protein level is decreased at most of them in unperturbed *nse3-R254E* and *smc6–74* mutants (Figure 7). Furthermore, accumulation of SMC5/6 was compromised on most loci in the *nse3-R254E* cells after HU or MMS treatment (Supplementary Figure S8), despite different mechanisms being involved in SMC5/6 localization after HU or MMS treatment (42). Therefore we speculate that the NSE3–DNA interaction is involved in general loading of the SMC5/6 complex on chromatin rather than in accumulation of the complex at specific chromosomal loci. Sub-to micromolar Kd values for the dsDNA and the other substrates (Figures 2 and 4; Supplementary Figures S4 and S6) are consistent with sequence non-specific binding and the loading function of the Nse3–DNA interaction (24).

The *smc6–74* mutation A151T is in a highly conserved arginine finger close to the ATP-binding site of the N-terminal globular domain (56) suggesting a defect in ATP binding/hydrolysis. Mutations within the ATP-binding pocket are lethal (28,55) similar to the lethal *nse3-R261E* mutation which disrupts Nse3–DNA interaction. The double mutation of *nse3-R254E* and *smc6–74* causes synthetic lethality (L. Jurcisinova, unpublished data). The phenotypic similarities between *nse3-R254E* and *smc6–74* mutants (Figure 6) and their synthetic lethality indicate that NSE3–DNA binding and SMC6 ATPase activity could play a role in the same essential function of the SMC5/6 complex.

It was previously shown that the ATPase activity of the whole *S. pombe* SMC5/6 complex is stimulated by dsDNA (28). Nevertheless, the *S. cerevisiae* Smc5 and Smc6 preferentially bind ssDNA (26,27), yet, ssDNA does not affect the rate of ATP hydrolysis (27,28). Based on our newly discovered NSE3–DNA binding mode, we speculate that the stimulation of the ATPase activity within the SMC5/6 complex might be mediated via the NSE1/3/4 sub-complex's interaction with dsDNA. Similar to condensin (24), binding of dsDNA to kleisin-associated NSE subunits may stimulate the ATPase activity of SMC5 and SMC6 head domains and direct dsDNA towards the SMC5/6 ring. Consistent with such a mechanism both *nse3-R254E* and *smc6–74* exhibit reduced chromatin association (Figure 7A).

Based on the similarities between SMC5/6 and the other SMC complexes (45), we propose a chromosome loading model (Figure 7B), which is similar to a proposed condensin model (24). In the first step, the NSE1/3/4 sub-complex binds to dsDNA. In the second step, we hypothesize that this interaction activates the SMC5/SMC6 ATPase cycle. This leads, in the third step, to topological loading of the SMC5/6 ring onto DNA. Addressing whether and how the DNA-binding of NSE1/3/4 sub-complex stimulates ATPase activity of the SMC core, how the ATP hydrolysis influences SMC5/6 complex loading onto chromatin fibers and whether and how the DNA fiber is loaded into the SMC5/6 ring, are questions for future research efforts. Although our hypothetical model needs to be tested further, our current data already suggest a critical role of the DNA-binding ability of the NSE1/3/4 sub-complex for SMC5/6 association with chromatin.

SUPPLEMENTARY DATA

Supplementary Data are available at NAR Online.

ACKNOWLEDGEMENTS

We thank R. Arribas, P. Kolesar, P.R. Potts, and V.V. Rogov, for expression constructs and purification protocols. M.N. Boddy, M. J. O'Connell, J.M. Murray, M. Prevorovsky, H. Shinagawa, and A. Watson, for yeast mutant strains and advice on ChIP assays. R. Bowater, I. Hickson, C. Hofr, T. Klumpler, I. Necasova, V. Pekarik, T. Shaikh, and S. Vidot are acknowledged for help with the NSE1/3/4–DNA binding analysis, and J. Fajkus for critical reading of the manuscript.

FUNDING

Medical Research Council Grant [G0501450]; Czech Science Foundation project [GA13-00774S to J.J.P.]; Cancer Research UK Programme Grant [C302/A14532 to A.W.O.]; CEITEC – Central European Institute of Technology [CZ.1.05/1.1.00/02.0068] funded from the European Regional Development Fund; European Social Funds [CZ.1.07/2.3.00/20.0189].

Conflict of interest statement. None declared.

REFERENCES

1. Losada,A. and Hirano,T. (2005) Dynamic molecular linkers of the genome: the first decade of SMC proteins. *Genes Dev.*, **19**, 1269–1287.
2. Carter,S.D. and Sjögren,C. (2012) The SMC complexes, DNA and chromosome topology: right or knot? *Crit. Rev. Biochem. Mol. Biol.*, **47**, 1–16.
3. Lehmann,A.R. (2005) The role of SMC proteins in the responses to DNA damage. *DNA Repair*, **4**, 309–314.
4. Wu,N. and Yu,H. (2012) The Smc complexes in DNA damage response. *Cell Biosci.*, **2**, 5.
5. Lehmann,A.R., Walicka,M., Griffiths,D.J., Murray,J.M., Watts,F.Z., McCready,S. and Carr,A.M. (1995) The rad18 gene of Schizosaccharomyces pombe defines a new subgroup of the SMC superfamily involved in DNA repair. *Mol. Cell. Biol.*, **15**, 7067–7080.
6. Ju,L., Wing,J., Taylor,E., Brandt,R., Slijepcevic,P., Horsch,M., Rathkolb,B., Rácz,I., Becker,L., Hans,W. *et al.* (2013) SMC6 is an essential gene in mice, but a hypomorphic mutant in the ATPase domain has a mild phenotype with a range of subtle abnormalities. *DNA Repair*, **12**, 356–366.
7. Irmisch,A., Ampatzidou,E., Mizuno,K., O'Connell,M.J. and Murray,J.M. (2009) Smc5/6 maintains stalled replication forks in a recombination-competent conformation. *EMBO J.*, **28**, 144–155.
8. Kegel,A. and Sjögren,C. (2010) The Smc5/6 Complex: More Than Repair? *Cold Spring Harb. Symp. Quant. Biol.*, **75**, 179–187.
9. Murray,J.M. and Carr,A.M. (2008) Smc5/6: a link between DNA repair and unidirectional replication? *Nat. Rev. Mol. Cell Biol.*, **9**, 177–182.
10. De Piccoli,G., Cortes-Ledesma,F., Ira,G., Torres-Rosell,J., Uhle,S., Farmer,S., Hwang,J.-Y., Machin,F., Ceschia,A., McAleenan,A. *et al.* (2006) Smc5–Smc6 mediate DNA double-strand-break repair by promoting sister-chromatid recombination. *Nat. Cell Biol.*, **8**, 1032–1034.
11. Sollier,J., Driscoll,R., Castellucci,F., Foiani,M., Jackson,S.P. and Branzei,D. (2009) The Saccharomyces cerevisiae Esc2 and Smc5–6 proteins promote sister chromatid junction-mediated intra-S repair. *Mol. Biol. Cell*, **20**, 1671–1682.
12. Copsey,A., Tang,S., Jordan,P.W., Blitzblau,H.G., Newcombe,S., Chan,A.C.-H., Newnham,L., Li,Z., Gray,S., Herbert,A.D. *et al.* (2013) Smc5/6 coordinates formation and resolution of joint molecules with chromosome morphology to ensure meiotic divisions. *PLoS Genet.*, **9**, e1004071.
13. Xaver,M., Huang,L., Chen,D. and Klein,F. (2013) Smc5/6-Mms21 Prevents and Eliminates Inappropriate Recombination Intermediates in Meiosis. *PLoS Genet.*, **9**, e1004067.
14. McAleenan,A., Cordon-Preciado,V., Clemente-Blanco,A., Liu,I.-C., Sen,N., Leonard,J., Jarmuz,A. and Aragón,L. (2012) SUMOylation of the α-kleisin subunit of cohesin is required for DNA damage-induced cohesion. *Curr. Biol.*, **22**, 1564–1575.
15. Outwin,E.A., Irmisch,A., Murray,J.M. and O'Connell,M.J. (2009) Smc5-Smc6-Dependent Removal of Cohesin from Mitotic Chromosomes. *Mol. Cell. Biol.*, **29**, 4363–4375.
16. Gallego-Paez,L.M., Tanaka,H., Bando,M., Takahashi,M., Nozaki,N., Nakato,R., Shirahige,K. and Hirota,T. (2014) Smc5/6-mediated regulation of replication progression contributes to chromosome assembly during mitosis in human cells. *Mol. Biol. Cell*, **25**, 302–317.
17. Potts,P.R. and Yu,H. (2007) The SMC5/6 complex maintains telomere length in ALT cancer cells through SUMOylation of telomere-binding proteins. *Nat. Struct. Mol. Biol.*, **14**, 581–590.
18. Cuylen,S., Metz,J. and Haering,C.H. (2011) Condensin structures chromosomal DNA through topological links. *Nat. Struct. Mol. Biol.*, **18**, 894–901.
19. Ivanov,D. and Nasmyth,K. (2005) A Topological Interaction between Cohesin Rings and a Circular Minichromosome. *Cell*, **122**, 849–860.
20. Arumugam,P., Gruber,S., Tanaka,K., Haering,C.H., Mechtler,K. and Nasmyth,K. (2003) ATP Hydrolysis Is Required for Cohesin's Association with Chromosomes. *Curr. Biol.*, **13**, 1941–1953.
21. Gruber,S., Arumugam,P., Katou,Y., Kuglitsch,D., Helmhart,W., Shirahige,K. and Nasmyth,K. (2006) Evidence that Loading of Cohesin Onto Chromosomes Involves Opening of Its SMC Hinge. *Cell*, **127**, 523–537.
22. Weitzer,S., Lehane,C. and Uhlmann,F. (2003) A Model for ATP Hydrolysis-Dependent Binding of Cohesin to DNA. *Curr. Biol.*, **13**, 1930–1940.
23. Murayama,Y. and Uhlmann,F. (2014) Biochemical reconstitution of topological DNA binding by the cohesin ring. *Nature*, **505**, 367–371.
24. Piazza,I., Rutkowska,A., Ori,A., Walczak,M., Metz,J., Pelechano,V., Beck,M. and Haering,C.H. (2014) Association of condensin with chromosomes depends on DNA binding by its HEAT-repeat subunits. *Nat. Struct. Mol. Biol.*, **21**, 560–568.
25. Griese,J.J., Witte,G. and Hopfner,K.-P. (2010) Structure and DNA binding activity of the mouse condensin hinge domain highlight common and diverse features of SMC proteins. *Nucleic Acids Res.*, **38**, 3454–3465.
26. Roy,M.-A. and D'Amours,D. (2011) DNA-binding properties of Smc6, a core component of the Smc5–6 DNA repair complex. *Biochem. Biophys. Res. Commun.*, **416**, 80–85.
27. Roy,M.-A., Siddiqui,N. and D'Amours,D. (2011) Dynamic and selective DNA-binding activity of Smc5, a core component of the Smc5-Smc6 complex. *Cell Cycle*, **10**, 690–700.
28. Fousteri,M.I. and Lehmann,A.R. (2000) A novel SMC protein complex in Schizosaccharomyces pombe contains the Rad18 DNA repair protein. *EMBO J.*, **19**, 1691–1702.
29. Palecek,J., Vidot,S., Feng,M., Doherty,A.J. and Lehmann,A.R. (2006) The Smc5-Smc6 DNA repair complex. bridging of the Smc5-Smc6 heads by the KLEISIN, Nse4, and non-Kleisin subunits. *J. Biol. Chem.*, **281**, 36952–36959.
30. Duan,X., Yang,Y., Chen,Y.-H., Arenz,J., Rangi,G.K., Zhao,X. and Ye,H. (2009) Architecture of the Smc5/6 Complex of Saccharomyces cerevisiae Reveals a Unique Interaction between the Nse5–6 Subcomplex and the Hinge Regions of Smc5 and Smc6. *J. Biol. Chem.*, **284**, 8507–8515.
31. Sergeant,J., Taylor,E., Palecek,J., Fousteri,M., Andrews,E.A., Sweeney,S., Shinagawa,H., Watts,F.Z. and Lehmann,A.R. (2005) Composition and Architecture of the Schizosaccharomyces pombe Rad18 (Smc5–6) Complex. *Mol. Cell. Biol.*, **25**, 172–184.
32. Hudson,J.J.R., Bednarova,K., Kozakova,L., Liao,C., Guerineau,M., Colnaghi,R., Vidot,S., Marek,J., Bathula,S.R., Lehmann,A.R. *et al.* (2011) Interactions between the Nse3 and Nse4 Components of the SMC5–6 Complex Identify Evolutionarily Conserved Interactions between MAGE and EID Families. *PLoS ONE*, **6**, e17270.
33. Doyle,J.M., Gao,J., Wang,J., Yang,M. and Potts,P.R. (2010) MAGE-RING Protein Complexes Comprise a Family of E3 Ubiquitin Ligases. *Mol. Cell*, **39**, 963–974.
34. Roy,A., Kucukural,A. and Zhang,Y. (2010) I-TASSER: a unified platform for automated protein structure and function prediction. *Nat. Protoc.*, **5**, 725–738.
35. Emsley,P. and Cowtan,K. (2004) *Coot*: model-building tools for molecular graphics. *Acta Crystallogr. D Biol. Crystallogr.*, **60**, 2126–2132.
36. de Vries,S.J., van Dijk,M. and Bonvin,A.M.J.J. (2010) The HADDOCK web server for data-driven biomolecular docking. *Nat. Protoc.*, **5**, 883–897.
37. Wassenaar,T.A., van Dijk,M., Loureiro-Ferreira,N., van der Schot,G., de Vries,S.J., Schmitz,C., van der Zwan,J., Boelens,R., Giachetti,A., Ferella,L. *et al.* (2012) WeNMR: Structural Biology on the Grid. *J. Grid Comput.*, **10**, 743–767.
38. Studier,F.W. (2005) Protein production by auto-induction in high density shaking cultures. *Protein Expr. Purif.*, **41**, 207–234.
39. Moreno,S., Klar,A. and Nurse,P. (1991) Molecular genetic analysis of fission yeast Schizosaccharomyces pombe. *Methods Enzymol.*, **194**, 795–823.

40. Morikawa,H., Morishita,T., Kawane,S., Iwasaki,H., Carr,A.M. and Shinagawa,H. (2004) Rad62 protein functionally and physically associates with the Smc5/Smc6 protein complex and is required for chromosome integrity and recombination repair in fission yeast. *Mol. Cell. Biol.*, **24**, 9401–9413.
41. Watson,A.T., Werler,P. and Carr,A.M. (2011) Regulation of gene expression at the fission yeast Schizosaccharomyces pombe urg1 locus. *Gene*, **484**, 75–85.
42. Pebernard,S., Schaffer,L., Campbell,D., Head,S.R. and Boddy,M.N. (2008) Localization of Smc5/6 to centromeres and telomeres requires heterochromatin and SUMO, respectively. *EMBO J.*, **27**, 3011–3023.
43. Guerineau,M., Kriz,Z., Kozakova,L., Bednarova,K., Janos,P. and Palecek,J. (2012) Analysis of the Nse3/MAGE-binding domain of the Nse4/EID family proteins. *PloS One*, **7**, e35813.
44. Kozakova,L., Vondrova,L., Stejskal,K., Charalabous,P., Kolesar,P., Lehmann,A.R., Uldrijan,S., Sanderson,C.M., Zdrahal,Z. and Palecek,J.J. (2015) The melanoma-associated antigen 1 (MAGEA1) protein stimulates the E3 ubiquitin-ligase activity of TRIM31 within a TRIM31-MAGEA1-NSE4 complex. *Cell Cycle*, **14**, 920–930.
45. Palecek,J.J. and Gruber,S.(2015) Kite proteins: A superfamily of SMC/kleisin partners conserved across bacteria, archaea and eukaryotes. *Structure*, in press.
46. Gajiwala,K.S. and Burley,S.K. (2000) Winged helix proteins. *Curr. Opin. Struct. Biol.*, **10**, 110–116.
47. Harami,G.M., Gyimesi,M. and Kovács,M. (2013) From keys to bulldozers: expanding roles for winged helix domains in nucleic-acid-binding proteins. *Trends Biochem. Sci.*, **38**, 364–371.
48. Ke,C., Humeniuk,M., S-Gracz,H. and Marszalek,P.E. (2007) Direct Measurements of Base Stacking Interactions in DNA by Single-Molecule Atomic-Force Spectroscopy. *Phys. Rev. Lett.*, **99**, 018302.
49. Cost,G.J. and Cozzarelli,N.R. (2006) Smc5p promotes faithful chromosome transmission and DNA repair in Saccharomyces cerevisiae. *Genetics*, **172**, 2185–2200.
50. Stephan,A.K., Kliszczak,M., Dodson,H., Cooley,C. and Morrison,C.G. (2011) Roles of vertebrate Smc5 in sister chromatid cohesion and homologous recombinational repair. *Mol. Cell. Biol.*, **31**, 1369–1381.
51. Pebernard,S., Wohlschlegel,J., McDonald,W.H., Yates,J.R. and Boddy,M.N. (2006) The Nse5-Nse6 dimer mediates DNA repair roles of the Smc5-Smc6 complex. *Mol. Cell. Biol.*, **26**, 1617–1630.
52. Bass,K.L., Murray,J.M. and O'Connell,M.J. (2012) Brc1-dependent recovery from replication stress. *J. Cell Sci.*, **125**, 2753–2764.
53. McDonald,W.H., Pavlova,Y., Yates,J.R. and Boddy,M.N. (2003) Novel essential DNA repair proteins Nse1 and Nse2 are subunits of the fission yeast Smc5-Smc6 complex. *J. Biol. Chem.*, **278**, 45460–45467.
54. Pebernard,S., McDonald,W.H., Pavlova,Y., Yates,J.R. and Boddy,M.N. (2004) Nse1, Nse2, and a novel subunit of the Smc5-Smc6 complex, Nse3, play a crucial role in meiosis. *Mol. Biol. Cell*, **15**, 4866–4876.
55. Verkade,H.M., Bugg,S.J., Lindsay,H.D., Carr,A.M. and O'Connell,M.J. (1999) Rad18 is required for DNA repair and checkpoint responses in fission yeast. *Mol. Biol. Cell*, **10**, 2905–2918.
56. Lammens,A., Schele,A. and Hopfner,K.-P. (2004) Structural biochemistry of ATP-driven dimerization and DNA-stimulated activation of SMC ATPases. *Curr. Biol.*, **14**, 1778–1782.